



Preparation and Characterization of Polyamide Thin Film Composite Nanofiltration Membrane Based on Polyurethane Nanofibrous Support

Mohsen Moslehi¹ · Hossein Mahdavi¹ · Aliakbar Ghaffari¹

Accepted: 11 January 2021 / Published online: 24 January 2021

© The Author(s), under exclusive licence to Springer Science+Business Media, LLC part of Springer Nature 2021

Abstract

Polyurethane nanofibers recognized to perform as a sub-layer were employed herein as a medial-layer of high porosity in the fabrication of a novel class of thin-film nanofiltration membranes. In line with the primary aim of high throughput production of PU electrospun nanofibrous membranes (ENMs) with different fiber sizes and proper morphologies, the needle-free electrospinning technique was employed. An interfacial polymerization procedure was also utilized to conveniently coat a polyamide (PA) thin film on the polyurethane ENMs. The effects of the nanofibrous interconnecting network, fiber size, pore size, and morphology on the NF performance were investigated. The nanofiltration performance including the separation of various salts, water flux, and the MWCO test were performed. The results implied that the fiber size decrement, nanofibers interconnection increment, as well as nanofibrous membrane pore size decrement, and the nanofibrous layer increment (with different fiber size) would lead the interfacial polymerization to perfection and obtaining a uniform PA thin layer. The salts rejection and water flux of Na_2SO_4 , MgSO_4 , MgCl_2 and NaCl were ($\sim 99 \pm 0.5\%$, $37 \pm 2.7 \text{ L/m}^2\text{h}$), ($\sim 98 \pm 1\%$, $40 \pm 1.5 \text{ L/m}^2\text{h}$), ($\sim 95 \pm 2\%$, $33 \pm 2 \text{ L/m}^2\text{h}$) and ($\sim 52 \pm 1\%$, $30 \pm 3 \text{ L/m}^2\text{h}$), respectively. In the final analysis, a comparison of filtration performance between PU nanofibrous NF membranes with other well-known nanofibrous NF membranes was conducted.

Keywords Needle-free electrospinning · Nanofiltration · Interfacial polymerization · Salt rejection

Introduction

New ways had to be found to develop the vital issue of novel filtration processes in the water treatment and the purification of various resources, i.e. surface water, groundwater, seawater, industrial wastewater, and/or peripheral contaminated water resources [1, 2]. The application of membrane-based processes has emerged as a topical state-of-the-art water purification technology and remarkable progress has been recently reported in terms of their utilization [3]. Nanofiltration (NF), as a pressure-driven procedure featuring both the advantages and utility of reverse osmosis (RO) and ultrafiltration (UF), have as yet been utilized in the water management field including the production of potable water, water softening, removal of micropollutants, as well as wastewater

treatment [4, 5]. The NF membrane process offers so many benefits such as lower required operating pressures, higher fluxes, and cost-effectiveness compared with those of RO membranes [6]. The major architecture employed in the fabrication of commercial NF membranes includes a thin-film composite (TFC) framework based on three layers involving (i) a non-woven polyester backing material, (ii) a microporous mid-layer cast or built on a non-woven fabric layer and (iii) a thin selective barrier polyamide layer. The interfacial polymerization (IP) technique is customarily the method of choice for the preparation of a thin selective barrier layer of TFC NF-membranes [7, 8]. Recently, tremendous efforts in research works have been devoted to excel the efficiency and filtration performance of the TFC membranes. However, the performance of conventional TFC membranes is restricted with water flux decline [9].

In light of this, the optimization of each layer in TFC membranes is quite essential for the enhancement of the filtration performance. Among which, the mid and active layer are the most influential ones for this purpose. In recent years, it was demonstrated in some studies that superseding

✉ Hossein Mahdavi
hmahdavi@khayam.ut.ac.ir

¹ School of Chemistry, College of Science, University of Tehran, P.O. Box 14155, 6455 Tehran, Iran

the second microporous mid-layer by a nanofibrous layer prepared by electrospinning technique would lead to the higher flux values in the novel class of TFC membranes so-called thin-film nanofibrous composite (TFNC) membrane in comparison with commercial membranes of the analogous rejection rate [10–13]. The reason for this increase in permeate flux is principally due to the generation of the water channels through the unique interface structure between the active layer and the nanofibers during interfacial polymerization [14]. The application context of electrospun nanofibrous mats involves such a broad domain extending from liquid phase water treatment, and air filtration to tissue engineering, and reinforced composites due to their proper interconnected nanofibrous networks and higher porosity [15–19]. As regards these characteristics, ENMs have come upon a remarkable situation in various filtration applications e.g. microfiltration (MF) [20, 21], UF [22], and NF [23]. Although ENMs have demonstrated their unique capabilities in the MF water treatment domain, the studies addressing the enhancement of their NF performance through a mid-layer appear to be relatively rare. The poor mechanical strength of the nanofibrous layer is amongst their major disadvantages in further applications. To tackle this problem, in most cases, heat pressing and thermal treatment methods have been used to increase the mechanical strength of the fibrous mats. Also, in most articles, a nozzle electrospinning technique has been used to make a nanofibrous sub-layer for the production of nanofiltration membranes. On the other hand, obstacles of the nozzle system, including nozzle clogging, low production rate, and the need for conditions monitoring are incompatible with the large-scale production of NF membranes [20–23].

In this study, a needle-free electrospinning technique was applied for the aim of preparing the ENMs with high throughput and the continuous production of nanofibrous mats. Moreover, the influential parameters in nanofibrous mid-layer morphology, i.e. nanofiber diameter, porosity, the interconnection of voids, nanofibrous membrane pore size, etc., on the thin layer and NF performance are investigated. Therefore, the distinction of present study is to prepare a nanofibrous mid-layer of high acceptability and sustainability using a needle-free method. What's more, thermoplastic polyurethane (TPU) presents a very high mechanical stability due to its elastomeric intrinsic which made it an attractive candidate for such broad research and application in the NF supporting layer. The nanofiber of TPU has thus been produced regarding its outstanding properties such as marvelous nanofibrous morphology, long-standing electrospinning capability, and unique mechanical properties [24, 25]. Thereby, the needle-free electrospinning set-up was utilized herein to fabricate electrospun nanofibrous PU mat as a mid-layer for TFNC-NF membranes. In this way, the electrospun nanofibrous PU was prepared along with an endeavor to

optimize the needle-free electrospinning parameters such as electrospinning technique, polymer concentration, and additives. Moreover, the effect of these parameters on the nanofibrous membranes was monitored. Ultimately, the TFNC-NF membranes were prepared through interfacial polymerization method upon one and two nanofibrous layers, and the impact of nanofibrous layer utilization was also evaluated.

Experimental

Materials

The thermoplastic elastomer polyurethane (Elastollan®1180A10) was purchased from BASF SE. Non-woven poly (ethylene terephthalate) (PET) substrate was obtained from Sanko, Japan, and employed as a baking material (BM). Tetrahydrofuran (THF), n-Hexane (99%), *N,N*-Dimethylformamide (DMF, 99.5%), *m*-phenylenediamine (MPD), trimesoyl chloride (TMC), triethylamine (TEA), sodium sulfate, magnesium chloride, and sodium chloride were purchased from Merck. Polyethylene glycol (PEG) with molecular weights of 200, 400, 600, and 1000 Da were purchased from Sigma-Aldrich.

Preparation of PU Nanofibrous Supports

As mentioned, a needle-free electrospinning method was employed to prepare PU ENMs as a sub-layer for TFNC-NF membranes, and the whole system is schematically depicted in Fig. 1. The positive pole of the high voltage power supply section was connected to two porous wires of a 500 mm length and 2 mm diameter. Likewise, the negative pole of high voltage was connected to the collector electrode plate of 650 mm length centered in the upper side of the nozzle electrodes. Moreover, the system was equipped with a scanning system of the polymeric solution with a scanning rate of 50 mm/s as well as wiry electrodes composed of two holders of 1L volume enabling reload-ability with either the same or different concentrations of the polymer. The take-up cylinder rate required for oscillating the PET as a BM was adjusted at 50 mm/s. The polymeric solutions of PU were prepared in concentrations of 12 and 5 w/v % at 50/50 v/v DMF/THF solvent mixture ratio at the ambient temperature. Besides, LiCl was utilized in the desired concentrations as a polymeric solution modifier. The other needle-free electrospinning conditions of PU ENMs preparation are presented in Table 1.

Preparation of TFNC-NF Membranes

After which the PU ENMs were prepared with the desired properties (i.e. convenient morphology, mechanical stability,

Table 1 Needle-free electrospinning settings

Applied voltage (kV)	120
The gulf between electrodes (cm)	22
Chamber temperature (°C)	24
Relative humidity (%)	45

and uniformity), the TFNC-NF membranes were fabricated via the interfacial polymerization built on these prepared nanofibrous membranes. Figure 2 depicts the two feasible pathways for the interfacial polymerization technique.

The phase sequence shifts in producing a thin layer would also lead to a metamorphosis in its quality and properties.

When the organic phase is added to the aqueous phase, the polymeric layer of a certain thickness is formed at the interface of the two phases. Conversely, when the aqueous phase is added to the organic phase, a thin layer is primarily formed in the interface with a phase displacement which then occurs due to the difference of density between the two phases. As a result, the phases are penetrated to one another causing the reaction media to shift into the aqueous phase during polymerization and the polymeric films remain in the aqueous phase. In this work, the method for the preparation of a thin selective polyamide layer on the surface of the nanofibrous mat was according to the Fig. 2b pathway. When the PU ENMs were immersed in the organic and subsequently in the aqueous phase, a phase shift takes place on

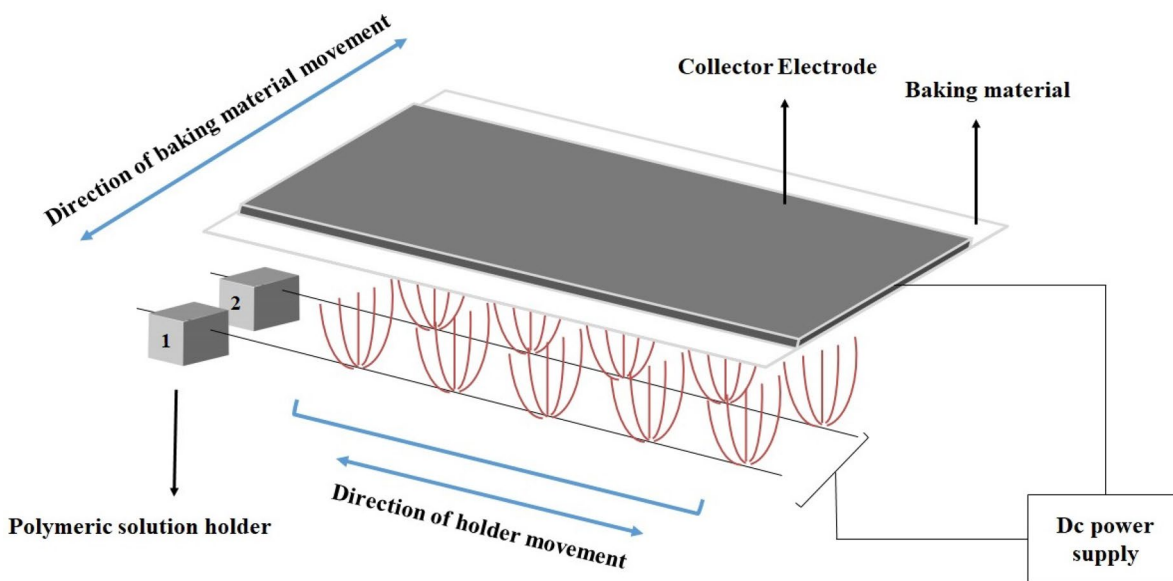


Fig. 1 Schematics of the wiry needle-free electrospinning system

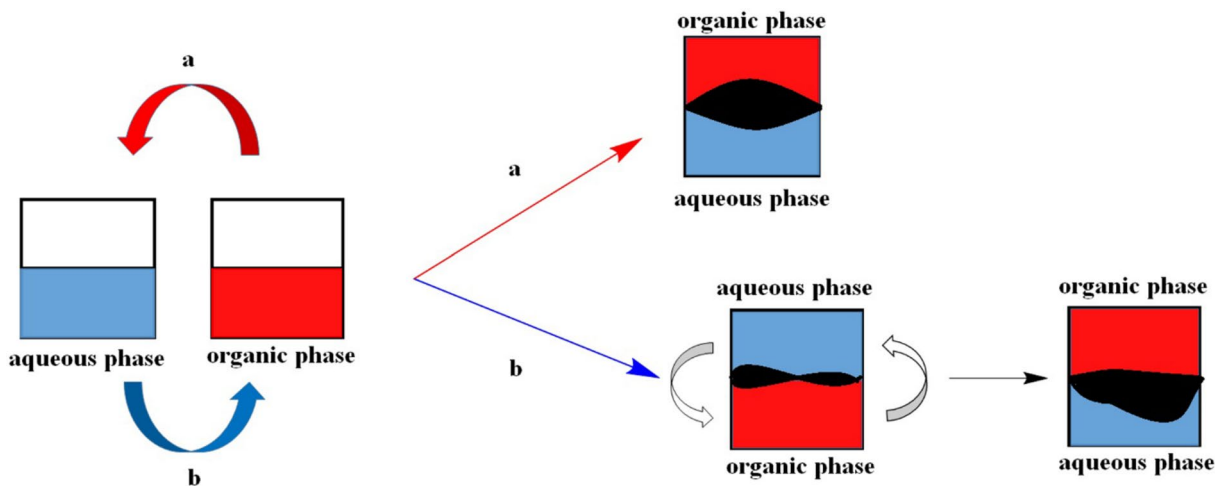


Fig. 2 Interfacial and reverse interfacial polymerization techniques

the membrane's surface which enables the polymeric thin film to infiltrate throughout the nanofibrous network leading to the enhancement of adhesion between sub-layer and thin film. Owing to the higher adhesion between these two layers and thus better permeation of the thin layer into the nanofibrous network, the nanocomposite architecture of the membrane becomes more dominant. This, in turn, would result in the improvement of water passage, flux, and performance for the nanofiltration membrane.

The reverse interfacial polymerization (IP-R) method utilized herein for the preparation of TFNC-NF membranes is according to the following test recipe: MPD (1.0% (w/v)) and TEA (1.0% (w/v)) were dissolved in water and TMC (0.1 (w/v)) was dissolved in hexane. Pre-cut PU nanofibrous layers (in the size of 7×7 cm) of a certain thickness were pasted on a clean dry glass container wrapped with adhesive tape. In the first step, nanofibrous support layers were impregnated by the organic phase for 3 min and then the solution was blotted from the sub-layers surface. In the following, they were sustained vertically for one minute and subsequently immersed in the aqueous solution for 2 min. The excess aqueous solution was also decanted after the polymerization. The resulting NF membranes were dried and cured at 87°C for 20 min and finally washed thoroughly with de-ionized water and kept in water before any further examination.

Characterizations

The morphology of all samples was investigated by scanning electron microscopy (SEM, JEOL, JSM-5600LV). For cross-sectional analysis, all samples were fractured in liquid nitrogen and the average fiber diameter of PU nanofibrous mats were measured from the SEM image analyzer software.

The porosity of sub-layers, as a criterion of nanofibrous density, was evaluated using the Eq. (1) [26]:

$$\text{Porosity} = [1 - (\rho'/\rho)] \times 100\% \quad (1)$$

in which ρ' and ρ represent the apparent and the bulk density of PU nanofibrous membrane, respectively. For this purpose, the apparent density of membrane samples with nearly 2 cm^2 and $130 \pm 12\ \mu\text{m}$ was calculated and the bulk density of PU granule was taken to be $1.11\ \text{g/cm}^3$. The porosity test was repeated three times and the average of which was reported. The total thickness of the nanofibrous sub-layer was determined using a micrometer. For the measurement of static water contact of thin-film nanofibrous composite nanofiltration membranes, advanced surface technologies, and data physics, the OCA 15 plus was applied. The mechanical study of PU nanofibrous membranes was performed using the Instron (the UK make 3345 Single Column Testing Systems). Besides, membranes in size of $1\text{ cm} \times 4\text{ cm}$ were applied for mechanical strength evaluation. The mean flow pore size and the bubble-point of the PU nanofibrous membranes were estimated employing a hand-made capillary flow porometer set-up (based on ASTM-F316-03) depicted in Fig. 3a [27]. The procedure of which the capillary flow porometer operates is as follows: initially, an inert gas, e.g. N_2 flows through a dry membrane and then through the same membrane after which it has been wetted by a wetter liquid. Ethyl alcohol with a defined surface tension of $22.3\ \text{dynes/cm}$ was utilized as the wetter agent [27]. Ultimately, after obtaining the data, the curves of gas flows versus pressure are plotted for dry and wet samples.

A typical wet, dry, and half-dry curve for a membrane sample is displayed in Fig. 4. The determination procedure of the largest pore and mean flow pore size from these curves is as follows. In the wet flow, the pores commence evacuating from

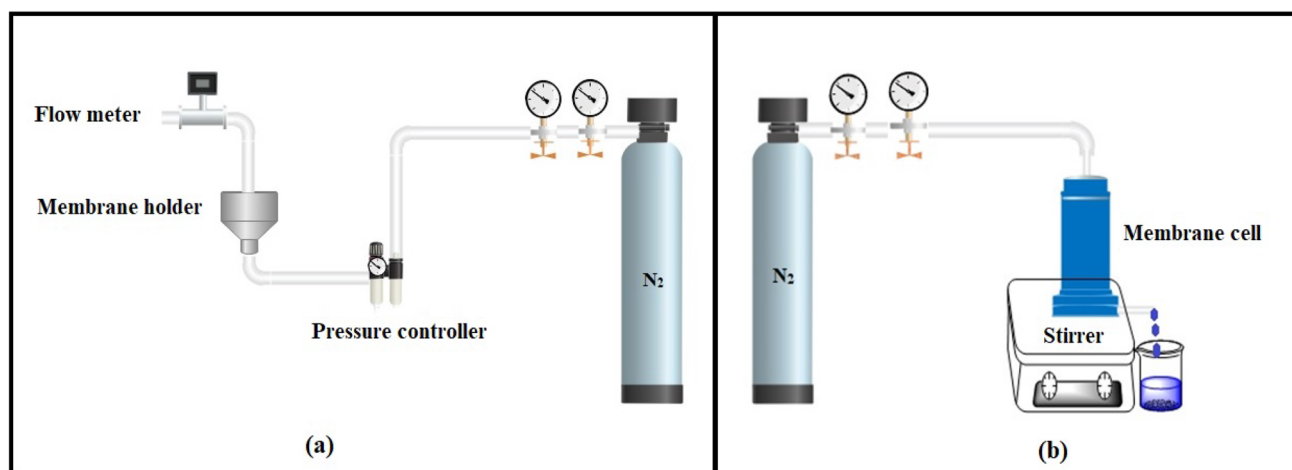


Fig. 3 a Pore size measurement set-up and b Separation and permeation set-up

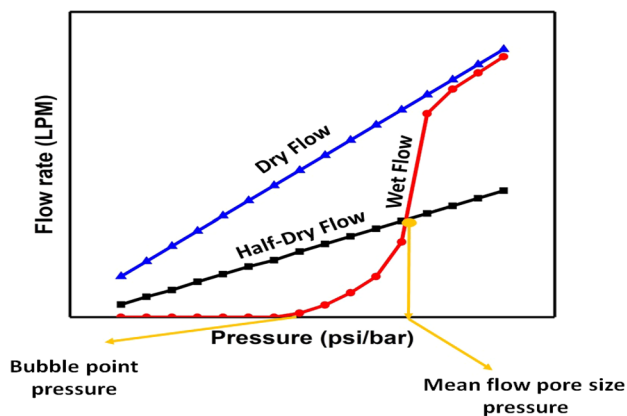


Fig. 4 Capillary flow porometry test for characterization of pore size and bubble point

the largest (bubble point) towards the smallest while the nitrogen gas pressure increases. Therefore, the pressure at which the increment of the wet flow initiates has corresponded to the largest pore, and that of the intersection of half-dry gas flow and wet flow is attributed to the mean flow pore size. The largest and mean flow pore sizes of the membranes were calculated from these mentioned pressures plotted in the curves applying the Eq. (2) [27]:

$$D = 2860\gamma\cos\theta/p \quad (2)$$

in which D is the membrane pore diameter (μm); θ the contact angle of the wetting agent; p the differential pressure (Pa); and γ is the surface tension of the wetting agent (dyn/cm). For the aim of this analysis, the membranes were cut into circular shapes of 4 cm diameter.

Nanofiltration Performance

The hand-made dead-end nanofiltration system possessing an active filtration area of $7.09 \times 10^{-4} \text{ m}^2$ was employed so as to evaluate the membrane performance (i.e. salt rejection and water flux) of TFNC-NF membranes which is schematically depicted in Fig. 3b. The TFNC-NF membranes were incised into the round shapes of the 4.5 cm diameter in a way that all membranes possessed a total thickness of $130 \pm 12 \mu\text{m}$. In the salt rejection measurement experiments, the concentration of salts as a feed aqueous solutions was 2000 ppm of Na_2SO_4 , MgCl_2 , and NaCl and the operating pressure for filtration was 5 bars. The collected permeate solution was weighed every 25 min and the value of feed and permeate solution conductivity was assessed using a conductivity meter (Extech-EC150).

The salt retention ($R\%$) was calculated through Eq. (3):

$$R = [1 - (C_P/C_F)] \times 100\% \quad (3)$$

in which C_P and C_F represent the conductivity of filtrate and feed solutions, respectively.

The pure water flux widely described as the representative of the energy consumption in the filtration as well as a practical method of comparing the permeability of different NF membranes was measured and reported in the volume of water permeate per time per area.

For TFNC-NF pore size characterization, a series of aqueous solutions comprising 1000 ppm PEG with different molecular weights of 200, 400, 600, and 1000 g/mol was utilized. In this manner, the aforementioned dead-end filtration cell operating in 5 bars pressure equipped with a total organic carbon analyzer (TOC, model Shimadzu TOC-5000) was utilized to determine the PEG concentrations in the permeate and feed solutions.

Results and Discussion

Pore Size Characterization of Nanofibrous Sub-layers

The dry flow, wet flow, and half-dry flow curves of PU nanofibrous sub-layer membranes were illustrated in Fig. 5, diagrams from which the membrane's pore characterizations could be realized. The diagram of Fig. 5a shows the data obtained from ENM-1 (i.e. 12 w/v% PU in a solvent mixture containing 50/50 v/v DMF/THF and 0.04 wt% LiCl). The pressure at which the wet flow has initiated is located at 0.12 bar and thus the largest pore was $5 \mu\text{m}$ calculated from the pore-pressure formula. Likewise, the pressure corresponding to the beginning of mean flow pore size was 0.65 bar and the correlated pore size was calculated to be $0.97 \mu\text{m}$. The bubble points as well as the mean flow pore size of ENM-2 prepared by 5 w/v% PU in the 50/50 v/v DMF/THF solvent mixture and 0.04 wt% LiCl, have been decreased as shown in Fig. 5b. This is due to the polymeric concentration drop during the electrospinning process which makes the fiber diameter and porosity to reduce and also the fiber density to increase. The bubble point and the correlating pressure to this point were $0.55 \mu\text{m}$ and 1.15 bar, respectively. Besides, its mean flow pore size was found to be $0.17 \mu\text{m}$ and the correlating pressure to this point has taken place at 3.75 bar.

Morphological Investigation of the Nanofibrous Membranes

The morphology properties of PU nanofibrous support prepared through needle-free electrospinning technique was evaluated by SEM technique. Amid the preparation way of these samples, the two holders of polymeric solution were charged by the same concentration of 12% wt PU in 50/50

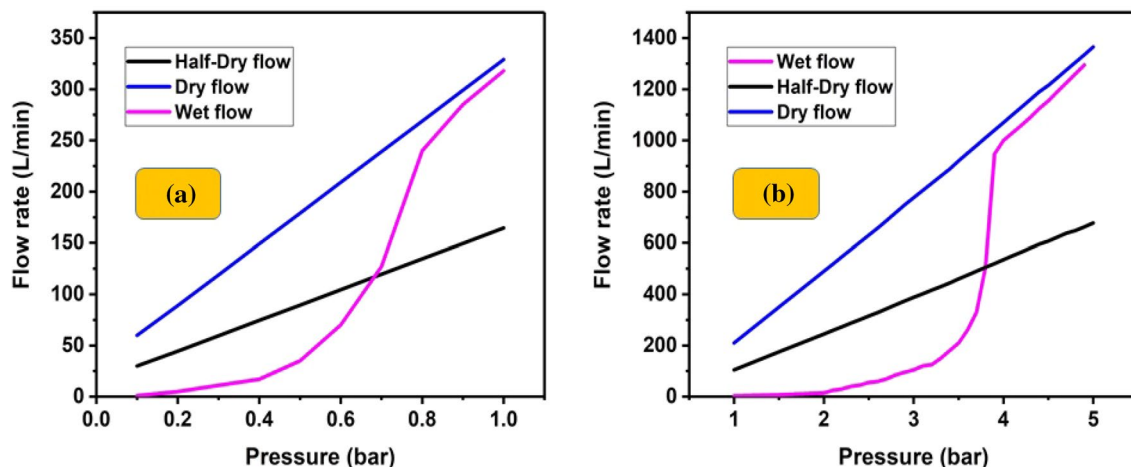


Fig. 5 The diagrams of pore-size measurements result using the capillary flow poro-meter method

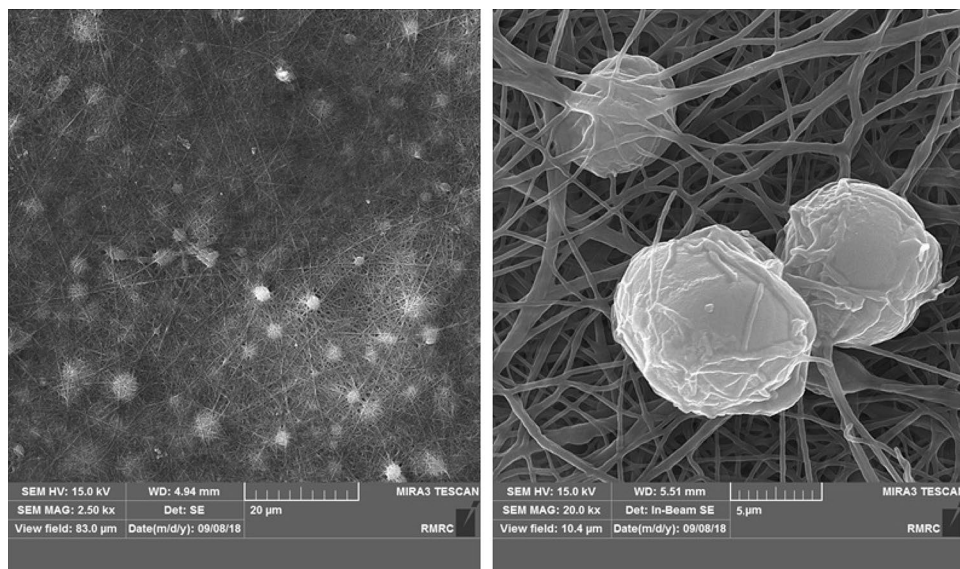
v/v DMF/THF, and thus the nanofibrous support with one layer having a concentration of 12% was produced. Figure 6 shows that the prepared electrospun nanofibrous membrane had a nanofibrous network with a non-uniform structure. Also, some beaded-fibers and beads and structure could be seen in this nanofibrous sub-layer. For this purpose, different methods have been utilized to produce nanofibers membrane with a uniform structure. One of the practical methods is to use different additives to improve the properties and morphology of nanofibers. In this work, LiCl was applied as an additive for the electrospinning solution.

In this way, for the preparation of nanofibrous membrane with a uniform structure, two holders of polymeric solution were charged by the same concentration of 12% wt PU in 50/50 v/v DMF/THF in the presence of 0.04% wt LiCl as a solution modifier (ENM-1) and thus the nanofibrous support

with one layer having a concentration of 12% was produced (Fig. 7). The adding of LiCl to the solution improved the polymeric solution conductivity which led to a higher needle-free electrospinning performance. This, in turn, enhanced the nanofibrous jets elongation and helped prevention of the beaded fiber formation. As a result, a uniform structure was obtained in which the average fiber diameter and porosity of PU nanofibrous sub-layers were 272 ± 7 nm and 86%, respectively.

The preparation of a nanofibrous sub-layer capable of meeting the required characteristics such as consistent morphology, fitting porosity, and excellent mechanical strength on the thin film formation during polymerization is a crucial step in the fabrication of TFNC-NF membranes. This sub-layer, which substantively serves as a mid-layer in the structure of TFNC-NF membranes, is also of paramount

Fig. 6 SEM images of PU ENM-1 (12% wt PU in 50/50 v/v DMF/THF)



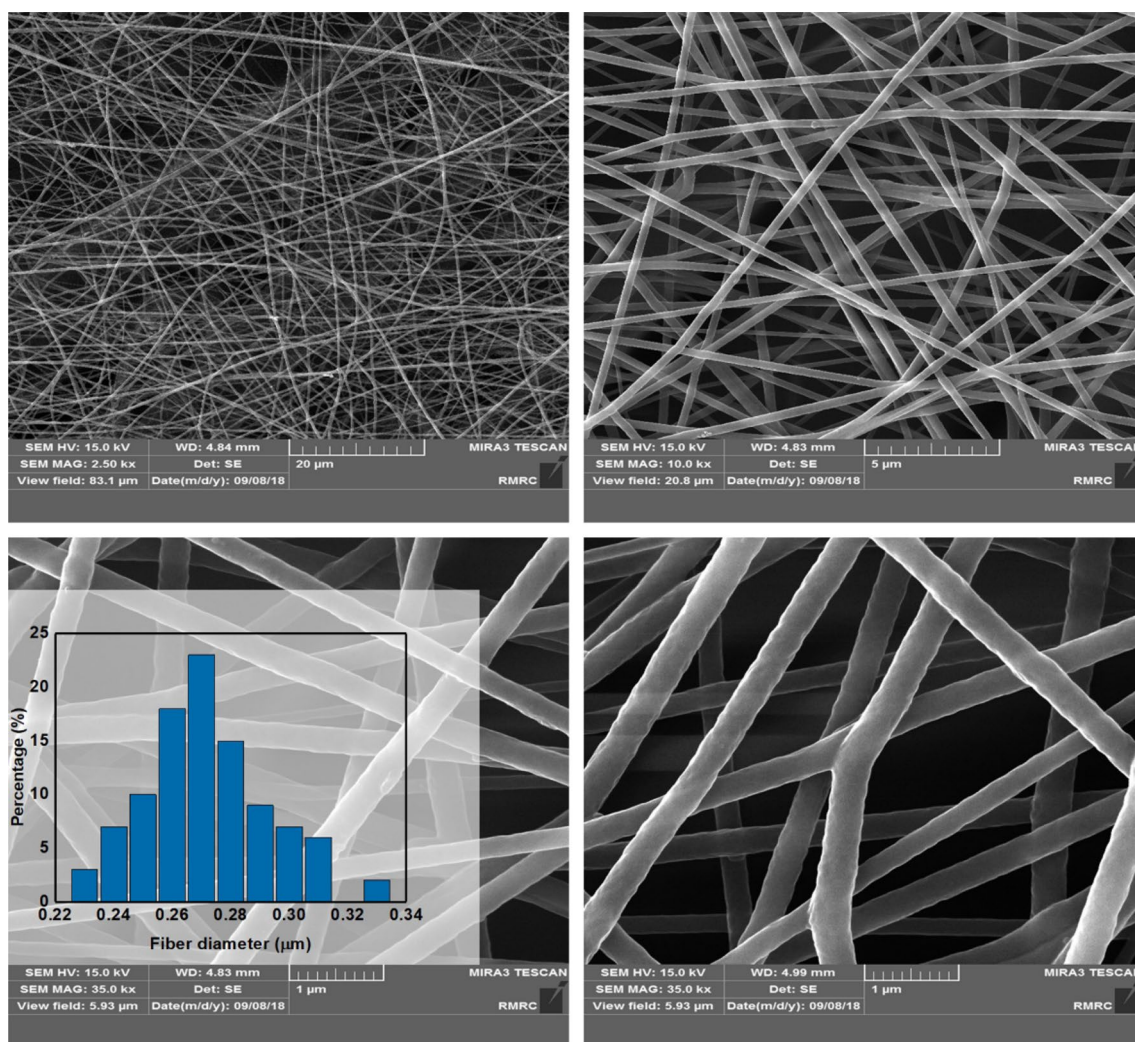


Fig. 7 SEM images of PU ENM-1 (12% wt PU in 50/50 v/v DMF/THF and 0.04% wt LiCl)

importance for the desired filtration performance besides the related pore size and morphology of the thin-film active layer. In line with this, the reverse interfacial polymerization technique was applied within NF production. The results of the evaluation of PU nanofibrous membranes (ENM-1) properties are illustrated in Fig. 6. The morphological characteristics of the TFNC membrane built on the mentioned nanofibrous sub-layer are shown in Fig. 8.

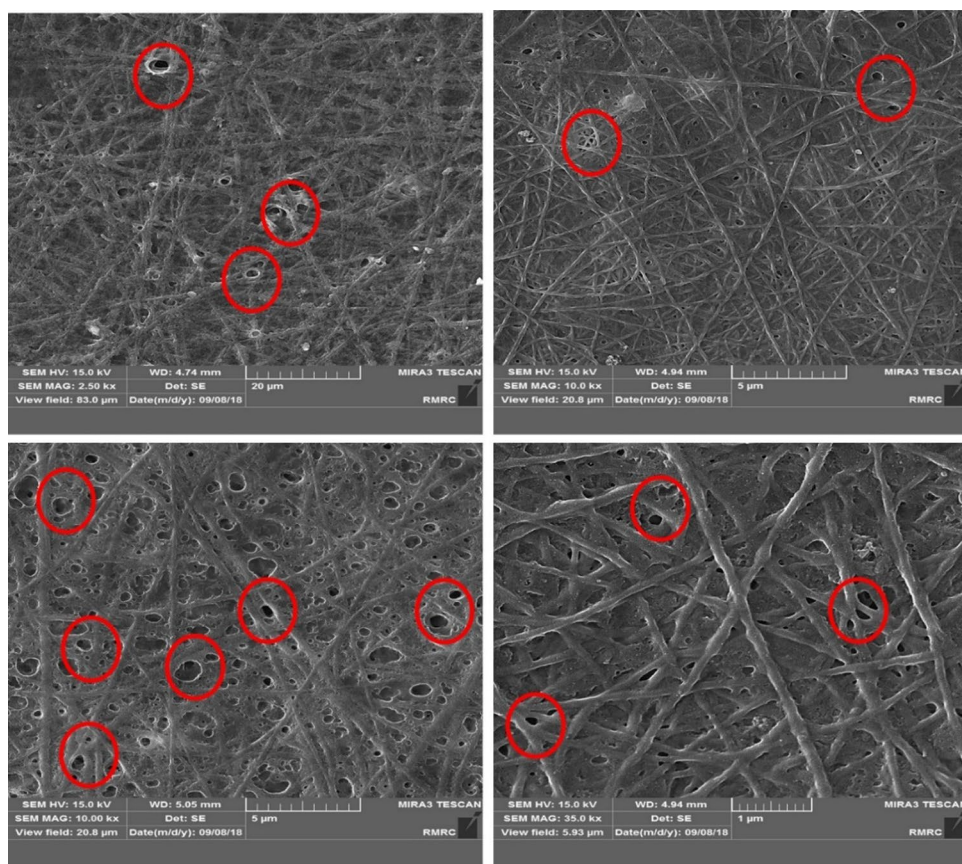
According to Fig. 8, an inhomogeneous composition of the PA layer on the ENM-1 sub-layer (having one nanofibrous layer) was observed which hindered the TFNC-1 membrane's propriety for NF application. The reason behind this could be due to the fiber's diameter and the related pore size enlargement which results in a defective coating of the polymeric active layer prepared from polymerization upon the nanofibrous sub-layer. Also, under the mentioned conditions, the density of the PA active layer could not meet the objects of NF filtration processes. In order to make great

strides in the thin active barrier layer and the preparation of a proper TFNC-NF membrane, the settings of the needle-free electrospinning technique (i.e. polymeric concentration and electrospinning procedure) were adjusted regarding the aim of continuous production of convenient nanofibrous sub-layers.

The SEM image of ENM-2 is illustrated in Fig. 9, in which the morphology betterment of this nanofibrous membrane compared to ENM-1 is crystal clear. During the preparation process of this sample, the two holders 1 and 2 were loaded with 12% w/v PU in 50/50 v/v DMF/THF solvent mixture with 0.04% wt LiCl as an additive and of the polymeric solution in the 5%w/v PU concentration in 50/50 v/v DMF/THF solvent mixture with 0.04% wt LiCl as an additive, respectively.

In this technical procedure, initially, the polymer in a higher concentration has been electrospun by the way of relocating the substrate to the front, thereafter so is the case

Fig. 8 SEM images of TFNC-NF-1 membrane based on ENM-1



for the polymer with different concentrations and properties. Therefore, the resultant nanofibrous membrane possesses three layers including (i) the sub-layer (a non-woven PET, a backing material), (ii) the mid-layer (nanofiber of 12%w/v PU in 50/50 v/v DMF/THF solvent mixture and 0.04%wt LiCl as an additive), and (iii) the top-layer (nanofiber with the concentration of 5%w/v PU, 50/50 v/v DMF/THF solvent mixture and 0.04% wt LiCl). This means that, on the polyester non-woven baking material, two nanofiber layers with different fiber sizes are formed. As indicated in the images, the geometrical morphology of the nanofibrous sub-layer was remarkably improved by the enrichment of the porosity and interconnection of the nanofibrous network. Moreover, the fiber diameter has been reduced (93 ± 5 nm, 78% and 272 ± 7 , 86% for ENM-2 and ENM-1, respectively) which is desirable for the NF performance. In this way, the reverse interfacial polymerization was applied for producing TFNC-NF membrane based on ENM-2 under the same procedure condition.

Figure 10 demonstrates the SEM images of the TFNC-NF-2 membrane. As remarked in the images, a suitable active layer was formed on the nanofibrous membrane surface and also throughout the membrane with high uniformity and reproducibility. Moreover, the layers are

free of defects and they thoroughly were coated and redistributed in the entire nanofibrous membrane structure. These results imply the fundamental role of nanofibrous sub-layer on the thin active layer and consequently on the TFNC-NF membrane of which has been built on thereof. As the nanofiber diameter was decreased, the related pore size was diminished and the polymerization process was accomplished more thoroughly. In consequence, the perfect and uniform active layer was obtained.

The SEM images of the TFNC-NF-2 membrane from yet other two viewpoints (top and cross-sectional) are exhibited in Fig. 11. Of the top view (left), the proper surface morphology of the nanofibers in TFNC membranes was manifestly discerned, and also the cross-sectional images (right) represented the formation of a uniform thin barrier layer of a thickness of 227 ± 11 nm on PU ENM-2. Focusing more elaborately on the cross-view, it is inferred that the polyamide thin layer and the reaction zone have shifted to a nanofibrous network due to the density disparity of the two phases as well as the nature of the IP-R method. As mentioned earlier, the drastic increase in the adhesion between the nanofibrous mat and the polyamide active layer could be the outcome of infiltration of polyamide thin films through the nanofibrous network.

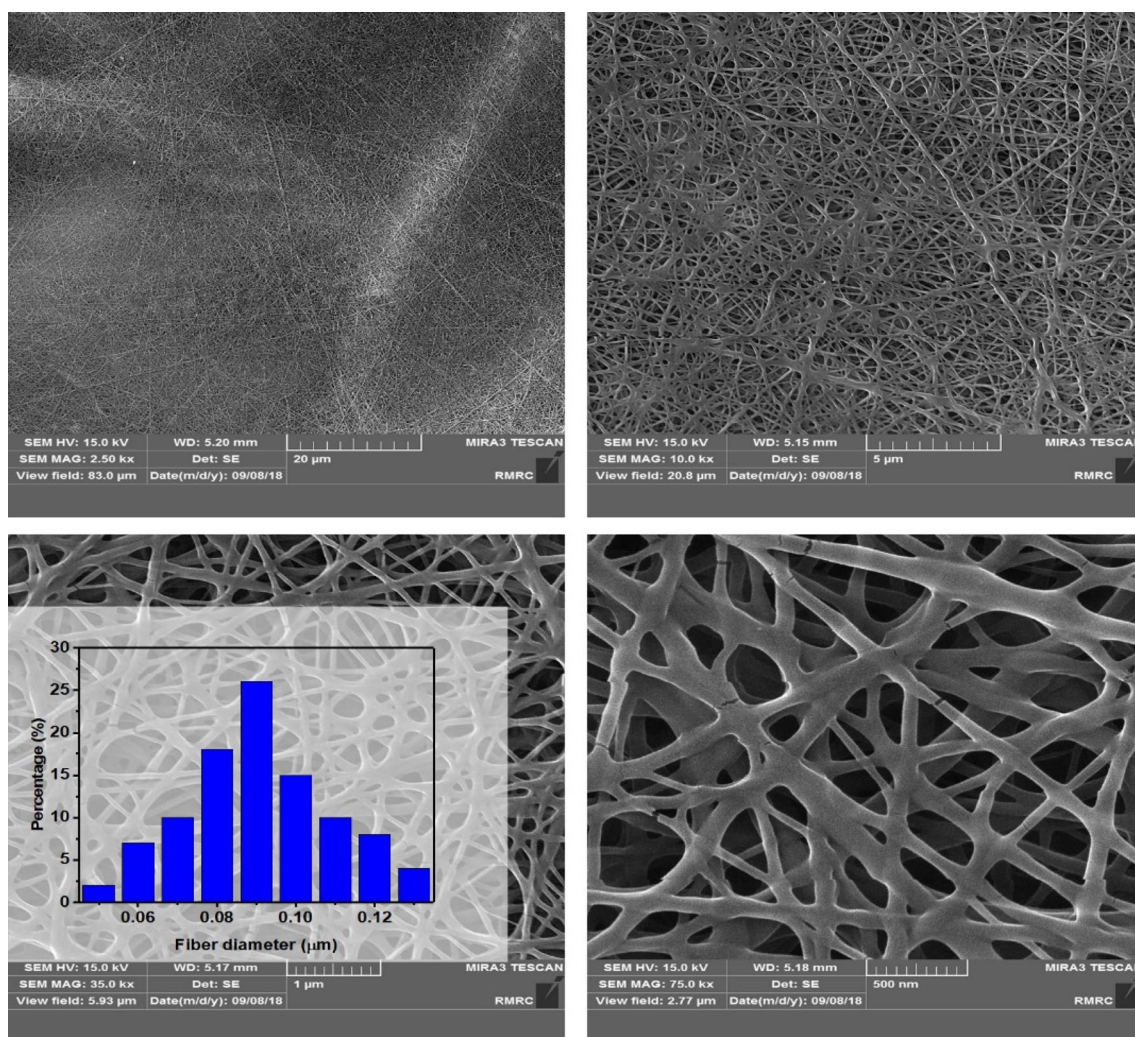


Fig. 9 SEM images of PU ENM-2 (5% wt PU in 50/50 v/v DMF/THF and 0.04% wt LiCl)

Nanofiltration Performance

The flux and rejection profile curves of TFNC-NF-2 in respect of Na_2SO_4 , MgSO_4 , MgCl_2 , and NaCl salts are shown in Figs. 12 and 13, respectively. As featured, the water flux for each feed solution was intensified while the pressure was increasing without any harsh pressure variation/drop. The nanofiber's fiber size decrement leads to the increment of the fibers packing density which, in turn, results in their pore-size decrement. The even pore-size distribution engendered a uniform thin film formation with the higher potential to adopt a cross-linked and compact structure. Thereby, a remarkable improvement in the mechanical properties of the NF membrane, as well as the adhesion between the nanofibrous network and the thin barrier layer, was achieved. The mentioned results demonstrate the sustainability of the TFNC-NF-2 membrane at various pressure ranges (4–10 bar).

Figure 12 shows the flux performance of the TFNC-2 NF membrane for pure water and other single salt solutions. As can be seen, the flux of pure water at different pressures is higher than that of other saline solutions. Because by adding of various salts to water, the osmotic pressure of the solution increased and this reduces the flux at different pressures compared to the pure water. Also, for different saline solutions, the permeate flux differ slightly from each other, which is due to the different osmotic pressures of solutions [28].

The hydrophobic and hydrophilic properties of a membrane play a fundamental role in its application in aqueous phase filtration. Case in point, utilization of a hydrophilic membrane in the water desalination processes is desired whereas, in the protein separation processes, membranes of more hydrophobicity are favorable to minimize protein adsorption and coagulation effects. To evaluate this property of the membrane, the water contact angle of the TFNC-NF-2

Fig. 10 SEM images of the TFNC-NF-2 membrane based upon ENM-2

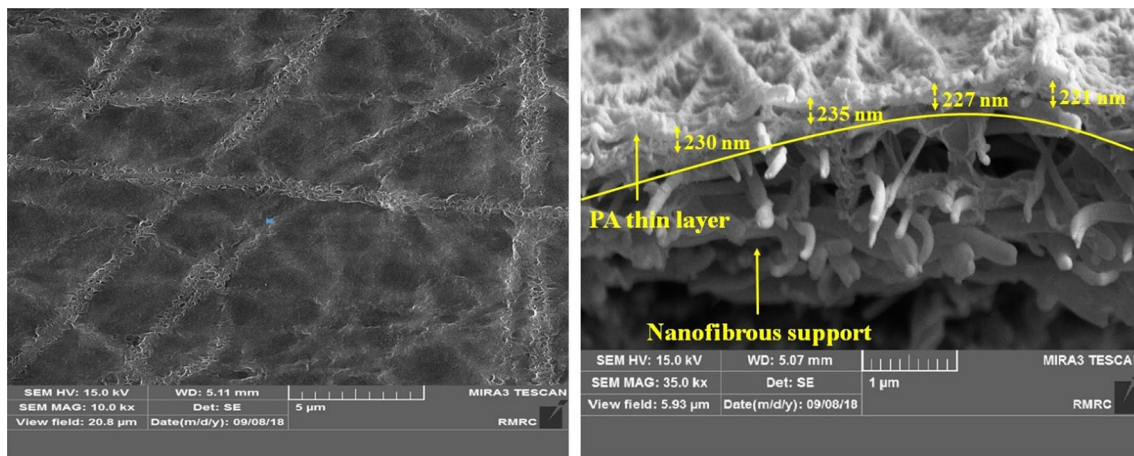
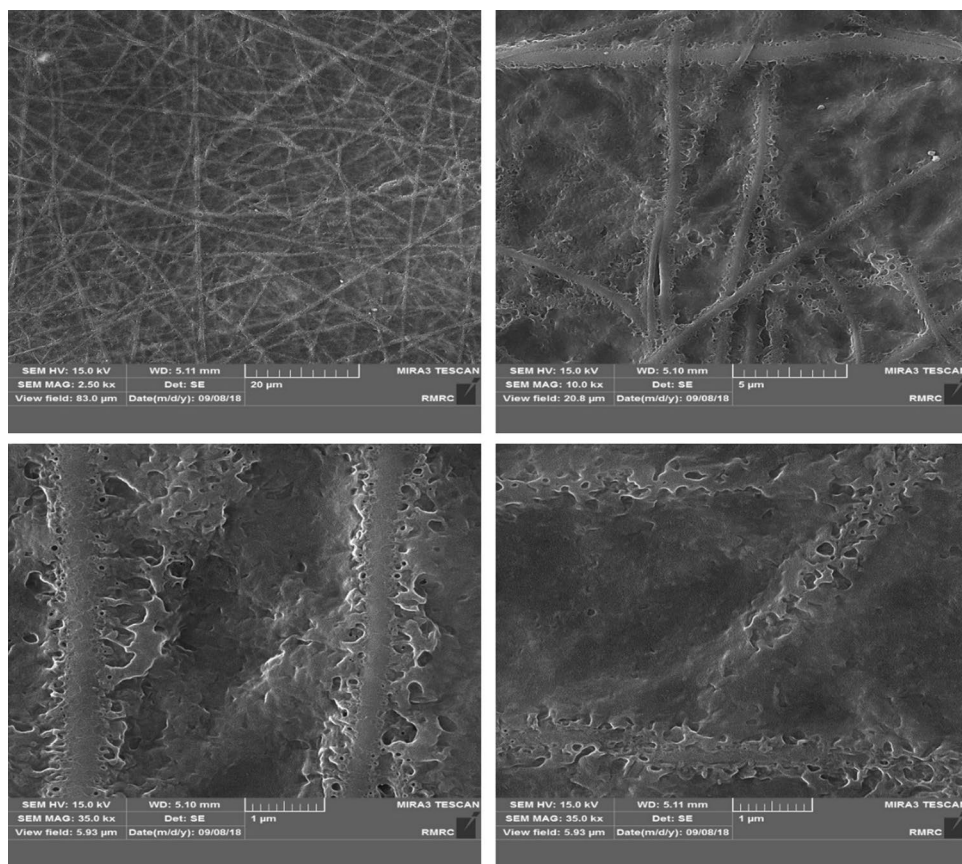


Fig. 11 Surface (left) and cross-section (right) views of TFNC-NF-2 membrane

membrane was measured and the results were represented in Fig. 12 (i.e. $\sim 29^\circ \pm 3$). This indicates the successful formation of the polyamide thin barrier layer on the PU nanofibrous sublayer via the IP-R method and also the compatibility of the product for NF applications.

The rejection performance of the nanofibrous NF membrane for different salts is shown in Fig. 13. Since the

water flux throughout the membrane is increased by the pressure increment effects, the solute flux is normally enhanced while its rejection remains changeless [29]. This behavior trend was also observed herein in which the flux and the salt rejection performance highly depending on the pore-size could be controlled and promoted via manipulating the nanofibrous sub-layer properties. The

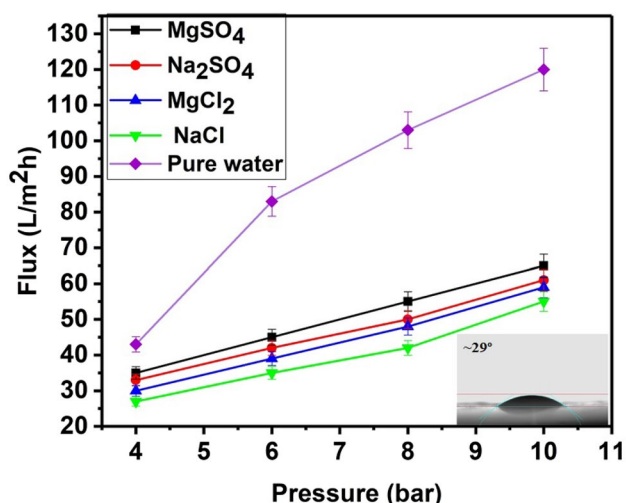


Fig. 12 Flux profile of TFNC-NF-2 membrane for different electrolytes and pure water

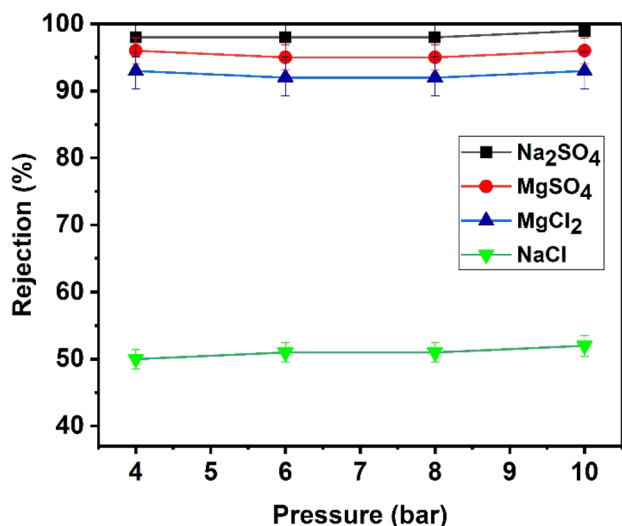


Fig. 13 Rejection profile of TFNC-NF-2 membrane for different electrolytes

basis for the operating mechanism of the salt separation phenomenon could conceivably be explained in two main strategies: (I) electric charge effect (Donnan effect) and (II) dielectric effect [30]. If presumably, the salt rejection is dominated by the electric charge effect, the order in the separation outcome, as observed often for other NF membranes, would become $\text{Na}_2\text{SO}_4 > \text{MgSO}_4 > \text{NaCl} > \text{MgCl}_2$ due to the presence of negative charges lying in the unreacted carboxyl groups of TMC. In other respect, when the second pathway (i.e. dielectric effect) dominates the rejection mechanism, the role of ionic valence would be fundamental. The divalent ions are, in a more forceful manner, repelled from the membrane

surface than that of the monovalent counterparts, irrespective of the charge character (i.e. positive or negative). Heretofore, the order of the electrolyte separation is expected to be $\text{MgSO}_4 > \text{Na}_2\text{SO}_4 \approx \text{MgCl}_2 > \text{NaCl}$. Surprisingly, the salt separation order herein was $\text{Na}_2\text{SO}_4 > \text{MgSO}_4 > \text{MgCl}_2 > \text{NaCl}$. In this regard, the electrical charge force lies behind the first half of the mentioned separation order whereas the other half of that is justified by the dielectric force as reported earlier [29]. Consequently, it could be suggested that both the charge and the dielectric repulsion effect account for the electrolyte separation.

For examining the mechanical stability of nanofibrous membranes, a tensile test was performed. Figure 14 illustrates the stress-strain diagram for the ENM-2 and TFNC-2 NF membranes. As shown from the image, the nanofibrous sub-layer represents acceptable mechanical integrity (3.9 Mpa stress and 120 % elongation). Moreover, the curves demonstrate that the tensile stress of the TFNC-2 NF membrane is increased from 3.9 to 4.7 MPa. These results suggest that reverse interfacial polymerization caused the penetration of polyamide active layer into nanofibrous network increasing the mechanical integrity of the NF membrane.

To evaluate the filtration constancy of thin-film nanofibrous composite NF membrane in practical conditions, long-term stability tests throughout water treatment was performed. As shown in Fig. 15, the TFNC-2 NF membrane exhibits proper performance during operation time. As implied by the results, nanofibrous membranes in proportion to their high mechanical strength have presented desired stability in the field of particle repulsion and flux as well. This indicates the realization of the fabrication of a new class of nanofibrous NF membranes for practicable applications.

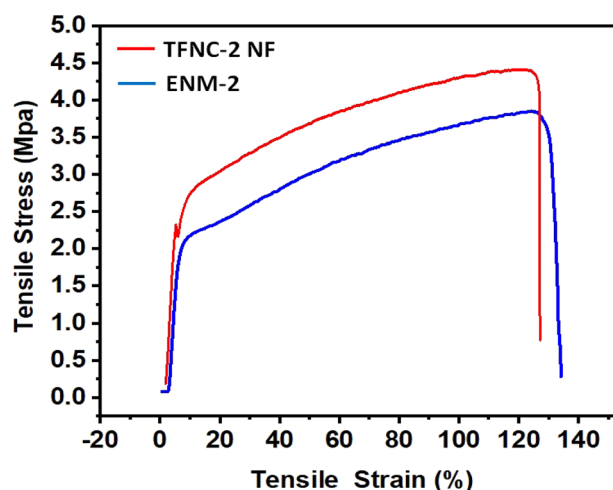


Fig. 14 Mechanical strength of PU ENM-2 and TFNC-2 NF membranes

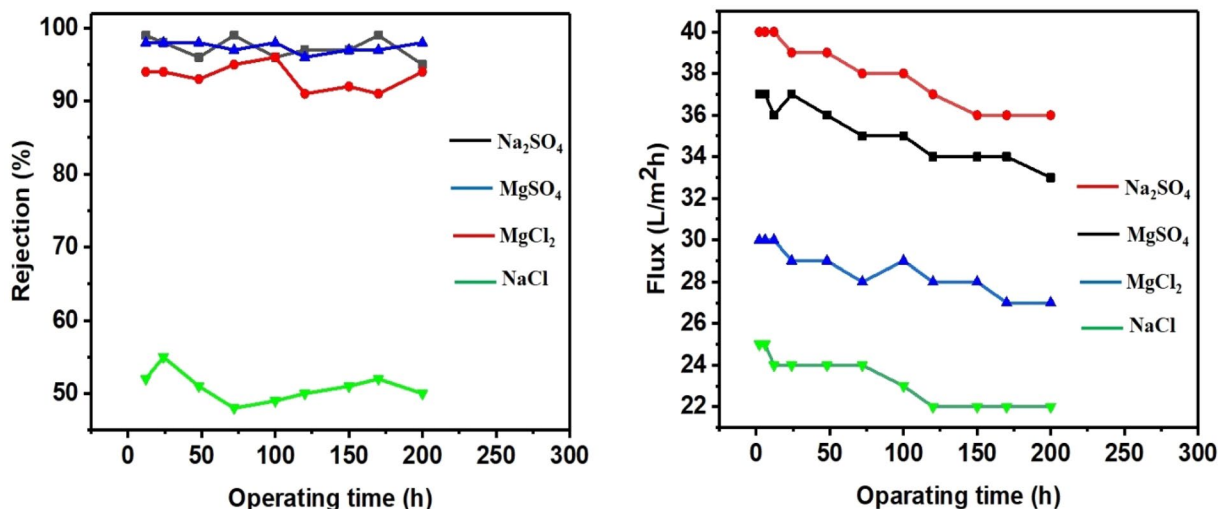


Fig. 15 The variation of solution flux and rejection of TFNC-2 NF membrane with operating time

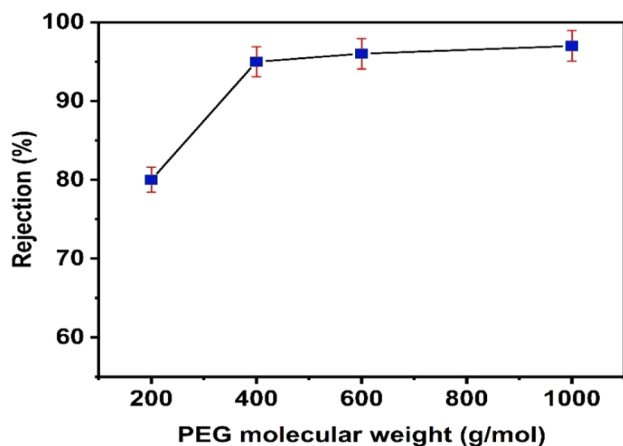


Fig. 16 PEG separation of TFNC-NF-2 membrane

Pore Size Measurement of Nanofiltration Membrane

The molecular weight cut-off (MWCO) results of the TFNC-2 NF-membrane are illustrated in Fig. 16. In this manner, PEG standard samples of the molecular weights with 200, 400, 600 and 1000 Da were employed in the MWCO testing as the standard test indicators. According to the results, the MWCO of the TFNC-2 NF-membrane was 400 Da in which the correlated rejection ratio was found to be $94 \pm 2\%$. On the other hand, the solution average diameter of PEG with related 200, 400, 600, and 1000 Da molecular weights were 1.3, 1.8, 2.1, and 2.7 nm, respectively [31]. Hence, the effective pore size of the TFNC-2 NF-membrane was around 1.8 nm.

Performance Comparison of TFNC-NF Membranes

A concise overview of the NF performances between the sample herein and the various nanofibrous thin-film nanofiltration membranes are tabulated in Table 2. In comparison between TFNC-2-NF^a and TFNC-4-NF^b membranes, it could be observed that the rejection of MgCl₂, NaCl and Na₂SO₄ salts and their flux were higher than that of TFNC-4-NF^b. In case of TFNC-2-NF^a and TFNC-4-NF^c, it is found that the rejection of MgCl₂, NaCl, Na₂SO₄ and MgSO₄ salts of TFNC-2-NF^a was higher than that of TFNC-4-NF^c and the electrolyte solution flux for each salt individually was also higher than that of TFNC-4-NF^c. For TFNC-2-NF^a and TFNC-NF^d, it can be concluded that their NaCl rejection is quite close to each other. However, the NaCl solution flux of TFNC-2-NF^a is markedly higher than that of TFNC-NF^d membrane. The reason behind this remarkable difference can be attributed to the PA thin-layer thickness employed in the NF of this study (227 ± 11 nm and $27 \mu\text{m}$ for TFNC-2-NF^a and TFNC-NF^d). At last, in the case of TFNC-2-NF^a and TFNC-2-NF^c, the rejection and permeate flux of MgSO₄ salt of TFNC-2-NF^a were higher than that of TFNC-2-NF^c. These results demonstrate the admissible and, in some cases, the superior performance of TFNC-2-NF^a nanofiltration membrane compared to the other nanofibrous counterparts.

Conclusions

Thin film nanofibrous composite NF membranes built upon TPU nanofibrous sub-layer, in which it was produced by means of high throughput needle-free electrospinning technique, were evaluated for water purification applications. Towards the aim of preparing a sub-layer having proper

Table 2 Comparative test results of salts rejection and water flux for various negatively charged nanofiltration

Membrane	R_{MgCl_2} (%)	R_{NaCl} (%)	$R_{Na_2SO_4}$ (%)	R_{MgSO_4} (%)	J_{MgCl_2} (L/m ² h)	J_{NaCl} (L/m ² h)	$J_{Na_2SO_4}$ (L/m ² h)	J_{MgSO_4} (L/m ² h)	Experimental conditions	References
TFNC-2-NF ^a	95 ± 2	52 ± 1	99 ± 0.5	98 ± 1	33 ± 2	30 ± 3	37 ± 2.7	40 ± 1.5	2000 ppm Na ₂ SO ₄ , 2000 ppm NaCl, 2000 ppm MgCl ₂ , 2000 ppm MgSO ₄ 5 bar	This study
TFNC-4-NF ^b	71 ± 2.5	78 ± 2	93 ± 3	–	21.5 ± 2	17 ± 0.5	25 ± 1.2	–	Dead-end set-up 2000 ppm Na ₂ SO ₄ , 2000 ppm NaCl, 2000 ppm MgCl ₂ , 5 bar	[23]
TFNC-4-NF ^c	~87	~57	~94	~92	~24	~22	~26	~30	Dead-end set-up 2000 ppm Na ₂ SO ₄ , 2000 ppm NaCl, 2000 ppm MgCl ₂ , 70 psig	[30]
TFNC-NF ^d	–	~67	–	–	–	~0.52	–	–	Cross-flow set-up 2000 ppm NaCl 70 psig	[32]
TFNC-2-NF ^e	–	–	–	~85 ± 4	–	–	–	–	Cross flow set-up 2000 ppm MgSO ₄ 70 psig Cross-flow set-up	[33]

^aPrepared via IP method (MPD (1w/v%) and TMC (0.1w/v%)) on PU/PET nanofibrous support^bPrepared via IP method (PPD(1w/v%) and TMC(0.3w/v%)) on PET self-support nanofibrous support^cPrepared via IP method (PPD(4w/v%) and TMC(0.3w/v%)) on PVDF self-support nanofibrous support^dPrepared via IP method (PIP(0.75w/v%), PPD(0.25w/v%) and TMC(0.1w/v%)) on PAN/PET nanofibrous support^ePrepared via IP method (PIP(0.7w/v%), BVP(0.3w/v%) and TMC(0.1w/v%)) on PAN/PET nanofibrous support.

morphology and properties, the concentration differential method was applied in the processes. Reverse interfacial polymerization procedure was employed on the surface of TPU ENM of different fiber sizes and nanofibrous layer.

The overall results of this study indicate that, the fiber size manipulation has resulted in the betterment of its properties including the porosity, the nanofibrous membrane pore size, the uniformity of thin barrier active layer, and the NF performance ultimately. However, one should consider the upper limit of the fiber-size and the pore-size enlargement since the ENMs having over-sized fibers are unable to serve as a supporting layer for the thin layer prepared via interfacial polymerization. Therefore, the formation of a uniform thin layer on the nanofibrous surface could be failed. In total, modification of the fiber-size and the morphology of the electrospun layer could offer several advantages towards the improvement of thin layer formation and enhance the rejection and fluxes in line with the water treatment applications.

References

- Shannon MA, Bohn PW, Elimelech M, Georgiadis JG, Marinas BJ, Mayes AM (2010) Science and technology for water purification in the coming decades. *World Sci*. <https://doi.org/10.1038/nature06599>
- Oki T, Kanae S (2006) Global hydrological cycles and world water resources. *Science* 313:1068–1072. <https://doi.org/10.1126/science.1128845>
- Ciardelli G, Corsi L, Marcucci M (2001) Membrane separation for wastewater reuse in the textile industry. *Resour Conserv Recycl* 31:189–197. [https://doi.org/10.1016/S0921-3449\(00\)00079-3](https://doi.org/10.1016/S0921-3449(00)00079-3)
- Van der Bruggen B, Everaert K, Wilms D, Vandecasteele C (2001) Application of nanofiltration for removal of pesticides, nitrate and hardness from ground water: rejection properties and economic evaluation. *J Membr Sci* 193:239–248. [https://doi.org/10.1016/S0376-7388\(01\)00517-8](https://doi.org/10.1016/S0376-7388(01)00517-8)
- Mondal S, Wickramasinghe SR (2008) Produced water treatment by nanofiltration and reverse osmosis membranes. *J Membr Sci* 322:162–170. <https://doi.org/10.1016/j.memsci.2008.05.039>
- Li Y, Su Y, Dong Y, Zhao X, Jiang Z, Zhang R, Zhao J (2014) Separation performance of thin-film composite nanofiltration membrane through interfacial polymerization using different amine monomers. *Desalination* 333:59–65. <https://doi.org/10.1016/j.desal.2013.11.035>
- Jeong BH, Hoek EM, Yan Y, Subramani A, Huang X, Hurwitz G, Ghosh AK, Jawor A (2007) Interfacial polymerization of thin film nanocomposites: a new concept for reverse osmosis membranes. *J Membr Sci* 294:1–7. <https://doi.org/10.1016/j.memsci.2007.02.025>
- Raaijmakers MJ, Benes NE (2016) Current trends in interfacial polymerization chemistry. *Prog Polym Sci* 63:86–142. <https://doi.org/10.1016/j.progpolymsci.2016.06.004>
- Lay WC, Zhang J, Tang C, Wang R, Liu Y, Fane AG (2012) Factors affecting flux performance of forward osmosis systems. *J Membr Sci* 394:151–168. <https://doi.org/10.1016/j.memsci.2011.12.035>
- Tang Z, Qiu C, McCutcheon JR, Yoon K, Ma H, Fang D, Lee E, Kopp C, Hsiao BS, Chu B (2009) Design and fabrication of electrospun polyethersulfone nanofibrous scaffold for high-flux nanofiltration membranes. *J Polym Sci Part B: Polym Phys* 47:2288–2300. <https://doi.org/10.1002/polb.21831>
- Wang X, Yeh TM, Wang Z, Yang R, Wang R, Ma H, Hsiao BS, Chu B (2014) Nanofiltration membranes prepared by interfacial polymerization on thin-film nanofibrous composite scaffold. *Polymer* 55:1358–1366. <https://doi.org/10.1016/j.polymer.2013.12.007>
- Xu GR, Liu XY, Xu JM, Li L, Su HC, Zhao HL, Feng HJ (2018) High flux nanofiltration membranes based on layer-by-layer assembly modified electrospun nanofibrous substrate. *Appl Surf Sci* 434:573–581. <https://doi.org/10.1016/j.apsusc.2017.10.188>
- Wang X, Ma H, Chu B, Hsiao BS (2017) Thin-film nanofibrous composite reverse osmosis membranes for desalination. *Desalination* 420:91–98. <https://doi.org/10.1016/j.desal.2017.06.029>
- Ma H, Burger C, Hsiao BS, Chu B (2012) Highly permeable polymer membranes containing directed channels for water purification. *ACS Publ* 1:723–726. <https://doi.org/10.1021/mz300163h>
- Liao Y, Loh CH, Tian M, Wang R, Fane AG (2018) Progress in electrospun polymeric nanofibrous membranes for water treatment: fabrication, modification and applications. *Prog Polym Sci* 77:69–94. <https://doi.org/10.1016/j.progpolymsci.2017.10.003>
- Zhu M, Han J, Wang F, Shao W, Xiong R, Zhang Q, Pan H, Yang Y, Samal SK, Zhang F (2017) Electrospun nanofibers membranes for effective air filtration. *Macromol Mater Eng* 302:1600353. <https://doi.org/10.1002/mame.201600353>
- Walser J, Ferguson SJ (2016) Oriented nanofibrous membranes for tissue engineering applications: electrospinning with secondary field control. *J Mech Behav Biomed Mater* 58:188–198. <https://doi.org/10.1016/j.jmbbm.2015.06.027>
- Zucchelli A, Focarete ML, Gualandi C, Ramakrishna S (2011) Electrospun nanofibers for enhancing structural performance of composite materials. *Polym Adv Technol* 22:339–349. <https://doi.org/10.1002/pat.1837>
- Bhardwaj N, Kundu SC (2010) Electrospinning: a fascinating fiber fabrication technique. *Biotechnol Adv* 28:325–347. <https://doi.org/10.1016/j.biotechadv.2010.01.004>
- Bae J, Baek I, Choi H (2016) Mechanically enhanced PES electrospun nanofiber membranes (ENMs) for microfiltration: The effects of ENM properties on membrane performance. *Water Res* 105:406–412. <https://doi.org/10.1016/j.watres.2016.09.020>
- Moslehi M, Mahdavi H (2019) Controlled pore size nanofibrous microfiltration membrane via multi-step interfacial polymerization: preparation and characterization. *Sep Purif Technol* 223:96–106. <https://doi.org/10.1016/j.seppur.2019.04.041>
- Dobosz KM, Kuo-Leblanc CA, Martin TJ, Schiffman JD (2017) Ultrafiltration membranes enhanced with electrospun nanofibers exhibit improved flux and fouling resistance. *Ind Eng Chem Res* 56:5724–5733. <https://doi.org/10.1021/acs.iecr.7b00631>
- Mahdavi H, Moslehi M (2016) A new thin film composite nanofiltration membrane based on pet nanofiber support and polyamide top layer: preparation and characterization. *J Polym Sci* 23:257. <https://doi.org/10.1007/s10965-016-1157-4>
- Erdem R, Usta I, Akalin M, Atak O, Yuksek M, Pars A (2015) The impact of solvent type and mixing ratios of solvents on the properties of polyurethane based electrospun nanofibers. *Appl Surf Sci* 334:227–230. <https://doi.org/10.1016/j.apsusc.2014.10.123>
- Gorji M, Jeddi AA, Gharehaghaji A (2012) Fabrication and characterization of polyurethane electrospun nanofiber membranes for protective clothing applications. *J Appl Polym Sci* 125:4135–4141. <https://doi.org/10.1002/app.36611>
- Li M, Wang D, Xiao R, Sun G, Zhao Q, Li H (2013) A novel high flux poly (trimethylene terephthalate) nanofiber membrane for microfiltration media. *Sep Purif Technol* 116:199–205. <https://doi.org/10.1016/j.seppur.2013.05.046>
- American Society for Testing and Materials. Committee D-19 on Water (2003) Standard test methods for pore size characteristics of

- membrane filters by bubble point and mean flow pore test. ASTM, West Conshohocken
28. Victor NJ, Borges CP, Ferraz HC (2016) Selective rejection of ions and correlation with surface properties of nanofiltration membranes. *Sep Purif Technol* 171:238–247. <https://doi.org/10.1016/j.seppur.2016.07.042>
 29. Pontalier PY, Ismail A, Ghoul M (1997) Mechanisms for the selective rejection of solutes in nanofiltration membranes. *Sep Purif Technol* 12:175–181. [https://doi.org/10.1016/S1383-5866\(97\)00047-6](https://doi.org/10.1016/S1383-5866(97)00047-6)
 30. Kaur S, Sundarrajan S, Rana D, Matsuura T, Ramakrishna S (2012) Influence of electrospun fiber size on the separation efficiency of thin film nanofiltration composite membrane. *J Membr Sci* 392:101–111. <https://doi.org/10.1016/j.memsci.2011.12.005>
 31. Lin J, Ladisch M, Patterson J, Noller C (1987) Determining pore size distribution in wet cellulose by measuring solute exclusion using a differential refractometer. *Biotechnol Bioeng* 29:976–981. <https://doi.org/10.1002/bit.260290809>
 32. Kaur S, Sundarrajan S, Gopal R, Ramakrishna S (2012) Formation and characterization of polyamide composite electrospun nanofibrous membranes for salt separation. *J Appl Polym Sci* 124:205–215. <https://doi.org/10.1002/app.36375>
 33. Kaur S, Barhate R, Sundarrajan S, Matsuura T, Ramakrishna S (2011) Hot pressing of electrospun membrane composite and its influence on separation performance on thin film composite nanofiltration membrane. *Desalination* 279:201–209. <https://doi.org/10.1016/j.desal.2011.06.009>

Publisher's note Springer Nature remains neutral with regard to jurisdictional claims in published maps and institutional affiliations.